Journal of Zhejiang University-SCIENCE C (Computers & Electronics)
ISSN 1869-1951 (Print); ISSN 1869-196X (Online)
www.zju.edu.cn/jzus; www.springerlink.com
E-mail: jzus@zju.edu.cn

Coupling analysis of transcutaneous energy transfer coils with planar sandwich structure for a novel artificial anal sphincter*

Lei KE†, Guo-zheng YAN, Sheng YAN, Zhi-wu WANG, Da-sheng LIU

(*Institute of Medical Precision Engineering and Intelligent Systems, School of Electronic Information and Electrical Engineering, Shanghai Jiao Tong University, Shanghai 200240, China*)

†E-mail: suda_kelei@163.com

Received Feb. 24, 2014; Revision accepted June 5, 2014; Crosschecked Oct. 16, 2014

Abstract: This paper presents a set of analytical expressions used to determine the coupling coefficient between primary and secondary Litz-wire planar coils used in a transcutaneous energy transfer (TET) system. A TET system has been designed to power a novel elastic scaling artificial anal sphincter system (ES-AASS) for treating severe fecal incontinence (FI), a condition that would benefit from an optimized TET. Expressions that describe the geometrical dimension dependence of self- and mutual inductances of planar coils on a ferrite substrate are provided. The effects of ferrite substrate conductivity, relative permeability, and geometrical dimensions are also considered. To verify these expressions, mutual coupling between planar coils is computed by 3D finite element analysis (FEA), and the proposed expressions show good agreement with numerical results. Different types of planar coils are fabricated with or without ferrite substrate. Measured results for each of the cases are compared with theoretical predictions and FEA solutions. The theoretical results and FEA results are in good agreement with the experimental data.

Key words: Transcutaneous energy transfer, Planar spiral inductance, Mutual inductance, Coupling coefficient, Artificial anal sphincter, Fecal incontinence

doi:10.1631/jzus.C1400062 **Document code:** A **CLC number:** TM15

1 Introduction

Fecal incontinence (FI) is a common clinical symptom that seriously affects patients' quality of life (QoL) (Bharucha *et al*., 2006). In recent years, an artificial bowel sphincter (ABS) (American Medical Systems, USA) has been developed as an alternative for patients with end-stage FI, and for whom conventional treatments or permanent colostomy had failed (Edden and Wexner, 2009). Despite its simplicity, it has some limitations. First, to open the occlusive cuff, patients must repeatedly squeeze and release the bulb of the control pump (placed under the scrotum or the labia major of the vulva), which may eventually damage their skin and possibly lead to infection. Second, because the cuff is refilled with fluid automatically, the time allotted for defecation is determined by the total duration of the refilling and opening of the cuff. Some patients do not have enough time to defecate and develop defecation difficulties after implantation due to the rapid closure of the cuff. Lastly, the pressure-regulating balloon may dilate or leak due to non-equilibrium osmotic pressure of the fillings. Under such conditions, cuff efficiency diminishes, which may lead to the recurrence of fecal incontinence (Mundy *et al*., 2004; Belyaev *et al*., 2006; Gallas *et al*., 2009). This paper describes part of our ongoing effort to realize an artificial anal sphincter, which is a novel mechanical elastic scaling muscle designed to overcome these drawbacks. The structure of this system, with sensor control, is described in detail in Section 2.

To reduce the potential risk of infection associated with wires through the skin, inductive

* Project supported by the National Natural Science Foundation of China (No. 31170968)

transcutaneous energy transfer (TET) technology was used to power the system without direct electrical connectivity (Zan *et al*., 2009a; 2009b). As an important part of a TET system, a secondary coil is implanted under the patient's skin, and a primary coil is placed on top of the secondary coil, outside the body. To estimate performance parameters of a TET system (efficiency, voltage gain, received voltage, etc.) or to optimize a power link (Jow and Ghovanloo, 2007; Ma *et al*., 2007; 2010; Lee and Lorenz, 2011; RamRakhyani *et al*., 2011; Zhang *et al*., 2011), requires the prediction of the quality factor of individual coils, and most importantly, the coupling coefficient—which can be represented by their self-inductance L and mutual inductance M between the coils. In the literature, analytical modeling of L for planar coils was well established. Three simple, approximate models that are based on a modified Wheeler formula, current sheets with uniform current distribution, and data-fitting techniques, were proposed by Mohan *et al*. (1999). Furthermore, complete physical modeling of on-chip planar coils was reported by Yue and Wong (2000). Compared with L, M depends on the shared magnetic field between the coils, and any variation in distance and misalignment of the coil pair can affect M, and thus inductive link performances as well. So, it is desirable to have a method to calculate M from the geometric parameters of the system. Various other approaches have been reported, most of which are based on the lookup table (Grover, 1962), numerical integration of elliptical functions (Babic *et al*., 2010; 2011), or Bessel functions (Zierhofer and Hochmair, 1996; Conway, 2007). Note that the inductance formulas presented in the above studies do not account for reflections from the ferrite substrate structure underneath. Such a layer will have an appreciable effect on the value of inductance.

In Section 3, we describe a further development of the models described in Hurley and Duffy (1997) and Acero *et al*. (2006a) by analyzing a spiral sandwiched inductor between two ferrite substrates with finite thickness. These models exhibit a high affinity with a planar coil pair TET system and some of these results can be applied. The characteristics of an air-cored structure and a primary-substrate structure are also considered. Some compact models for predicting L and M are presented. The proposed models calculate the prediction based on the winding characteristics, substrate properties, geometric parameters of the planar coils, as well as the relative placement of the coils in the TET system. Thus, the proposed mutual inductance model will enable the analytical prediction of the performance parameters of TET systems and their optimization.

The accuracy of these expressions is evaluated in two ways: with field solver simulations and with measurement data. For simulations, we use 3D finite element analysis (FEA) with ANSYS Maxwell software described in Section 4. A very accurate numerical solution is obtained for the design of coils and transformers (ANSYS, Inc., 2006). Two types of primary coils and four types of secondary coils with or without ferrite substrate are fabricated. The mutual inductance of three kinds of coil is measured, and then the coupling coefficient between them is calculated in relation to the self-inductance of the coil. Theoretical and FEA results are compared to the measured data in Section 5. Finally, some conclusions are presented in Section 6.

2 The novel artificial anal sphincter system

The new version of an artificial anal sphincter system (AASS) with biosensor feedback powered by a TET system is an integrative, modular, and remote-controlled sphincter prosthesis that comprises mainly three modules: an internal artificial anal sphincter (IAAS), a TET system, and an external controller.

The novel elastic scaling artificial anal sphincter prosthesis (ES-AASP) is composed of an annular elastic mechanism and a shrinkable actuator (Fig. 1a). The actuator integrates a steel wire rope, a windlass wheel, a worm gear box, and a micromotor. The annular elastic mechanism consists of springs encapsulated in medical silica gel bellows, and the end of the spring is fixed on both sides of the worm gear box. A steel wire runs through the worm gear box and springs via a windlass wheel, and connects with a button-type structure at the end of the springs. The micromotor drives the worm gears and windlass wheel. The stretch of the spring mechanism is realized by retracting and loosening the steel wire rope, so that the inner diameter can be changed and equidistant shrinkage in the radial direction can be realized to

achieve the shrinkage and release of the intestinal canal. The inner diameter of the annular spring can be maintained at any size by using the self-locking function of the worm and gear structure. The button-type structure at the end of the spring guarantees that the prosthesis implant can be accomplished without the need for rectum anastomosis. A diaphragm-typed biological pressure sensor (0.2-mm thick) was mounted in the wall of the worm. Worm gear box was used to control the degree of contraction of the spring to ensure that excrement can be kept within the pressure range for safety clamping, and to prevent ischemic necrosis of the intestinal wall caused by excessive pressure. In the actual design, the occlusion pressure threshold was set between 4.05 and 7.16 kPa, which ensures that the risk of ischemic injury to the bowel is minimal (Wong *et al*., 2002; Zan *et al*., 2008). The acting surface on the intestinal wall is enlarged by adopting a square spring to reduce its thickness in the radial direction and the volume simultaneously. The length of the spring can be changed according to the specific size of the enteric cavity. The total power consumption of the system is no more than 800 mW for any action or attitude. We fabricated a set of prototypes as shown in Figs. 1c and 1d. The ES-AASP can be compressed or relaxed, and thus the state of continence can be controlled by the internal driver unit (Fig. 1b).

The remaining components of the ES-AASP were encapsulated in biocompatible-grade silicon so that the device is suitable for implantation. During implantation, the prosthesis was placed around the end of the rectum, the driver unit was fixed in a subcutaneous pouch in the left abdominal wall, and the energy-receiving coil was embedded in a subcutaneous area of the lower back on one side, and connected to the driver unit by a subcutaneous wire tunneled through the peritoneum.

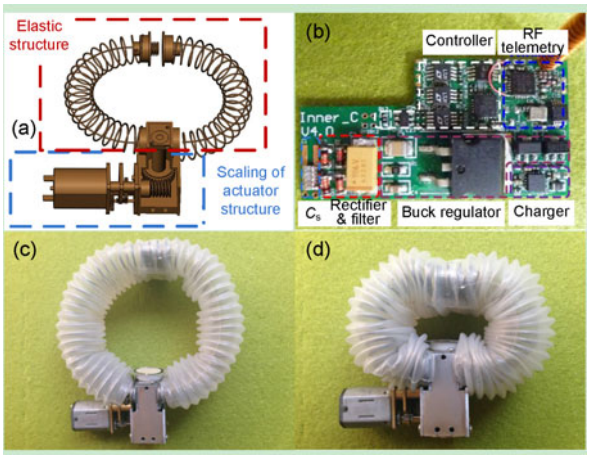

Fig. 1 Novel ES-AASP prototype

(a) CAD design of the elastic scaling artificial sphincter prosthesis; (b) Implanted driver unit; New sphincter prosthesis cuff with sensor: Relaxed=Defecation (c) and Compressed=Continence (d)

3 Coupling analysis of the TET coil pair

3.1 Structure of Litz-wire planar coil

There are two main types of air-cored coil designs: planar spiral coil and solenoid coil. In a planar spiral coil, the wire is concentrated in the middle whereas, in a solenoid coil, the wire is concentrated towards the edge of the coil. Compared with solenoid coils, planar spiral coils have advantages in applications in which the size of the coil is critical. These coils can be very thin, and about the thickness of the Litz wire being used, which makes them ideal for implantation under the skin. Thus, a planar spiral coil is selected for the TET application. Note that the mutual inductance between the primary and secondary coils is an important parameter in a TET system, which determines its capacity and efficiency. To quantify the differences in coupling between various coil designs, four different designs based on air-cored and substrate coil configurations are analyzed (Fig. 2). Figs. 2a and 2d are the standard air-cored and sandwich coils, respectively. The self-inductance L and mutual inductance M of the different designs, and the

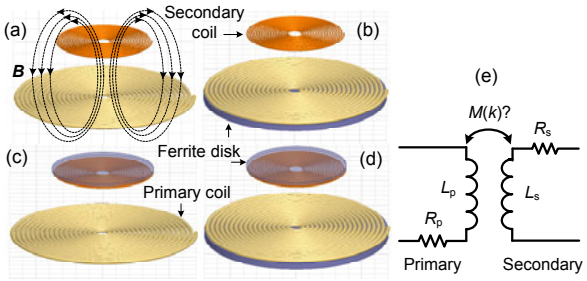

Fig. 2 Various primary and secondary coil designs

(a) Air-cored structure design; (b) Primary-substrate structure design; (c) Secondary-substrate structure design; (d) Sandwich structure design; (e) Link model. R_p and L_p are the series resistance and inductance of the primary coil, respectively. R_s and L_s are the series resistance and inductance of the secondary coil, respectively. $\boldsymbol{B}$ is the primary magnetic flux density

enhancement effect of a ferrite substrate of magnetic permeability μ_r, electrical conductivity σ, and thickness t on L and M are analyzed based on analytical models, experimental measurements, and simulations carried out in ANSYS. This is also done to ensure the practicality of the design. The external radius of coils (R_{out}) is the same in each design. However, the internal radius of coils (R_{in}), varies depending on the design of the secondary coil.

3.2 Air-cored structure

TET is based on mutual magnetic coupling between the pair of coils. Mutual inductance M is a measure of the extent of magnetic linkage between current-carrying coils. The M between these two coils primarily depends on the geometric parameters of the inductors and their relative placement.

Following Zierhofer and Hochmair (1996), the mutual inductance of two parallel single-turn air-cored coils with a loop radius of r and a, respectively, can be expressed by Eq. (1), assuming that the ratios R/r and R/a are sufficiently small, where R, d, and ρ are the wire radius, relative axial separation, and lateral misalignment respectively, between the two coils.

$$M(a,r,\rho,d)=\pi\mu_0\sqrt{ar}\int_0^{\infty}J_1(x\sqrt{a/r})J_1(x\sqrt{r/a})\cdot J_0\left(x\frac{\rho}{\sqrt{ar}}\right)\exp\left(-x\frac{d}{\sqrt{ar}}\right)\mathrm{d}x, \quad (1)$$

where J_0 and J_1 are the Bessel functions of zero and first orders respectively, and μ_0 is the vacuum permeability.

For perfectly aligned loops where ρ=0, the mutual inductance between the coils can be simplified to

$$M_0(a,r,\rho=0,d)=\mu_0\sqrt{ar}\left[\left(\frac{2}{k}-k\right)K(k)-\frac{2}{k}E(k)\right], \quad (2)$$

where

$$k=\sqrt{\frac{4ar}{(a+r)^2+d^2}}, \quad (3)$$

and $K(k)$ and $E(k)$ are the complete elliptic integrals of the first and second kinds, respectively (Soma *et al*., 1987; Zierhofer and Hochmair, 1996).

Self-inductance is the ratio of flux linkage to current in one coil. As shown by Zierhofer and Hochmair (1996), for the condition $R/a\ll1$, the self-inductance of a coil with loop radius a and wire radius R can be approximated as

$$L_0(a,R)=\mu_0 a\left(\ln\frac{8a}{R}-2\right). \quad (4)$$

As mentioned above, primary and secondary coils used in a TET system usually consist of a multi-turn of single circular loops of about equal diameter. In Fig. 3, the primary and secondary Litz-wire coils consist of N_a and N_r Litz-wire concentric turns, each one of which is with a radius of a_i or r_j, respectively. The self-inductance of such coils is approximately equal to the sum of the self-inductance of the individual concentric single loops and the partial mutual inductance between every turn on the coil. For a coil composed of N_a concentric circular loops with different radii a_i (i=1, 2, ... , N_a) and with wire radius R, the overall self-inductance L can be approximated by

$$L=\sum_{i=1}^{N_a}\sum_{j=1}^{N_a}M_0(a_i,a_j,\rho=0,d=0)(1-\delta_{ij})+\sum_{i=1}^{N_a}L_0(a_i,R), \quad (5)$$

where δ_{ij}=1 for i=j and δ_{ij}=0 otherwise.

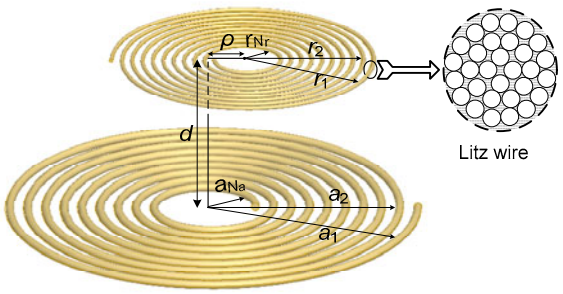

Fig. 3 Geometric arrangement of, and notation for, primary and secondary air-cored planar coils composed of Litz wire

Based on the mutual inductance between a pair of single loops in parallel planes, the overall mutual inductance M between the primary and secondary

coils can be calculated by summing the partial mutual inductance values between every turn on one coil and all of the turns on the other coils:

$$M=\sum_{i=1}^{N_a}\sum_{j=1}^{N_r}M_0(a_i,r_j,\rho,d). \tag{6}$$

3.3 Primary-substrate structure

Fig. 4 shows a schematic diagram of planar coils in a primary-substrate structure design in TET inductive link. The secondary coil consists of an N_r-turn planar winding with loop radius r_i (i=1, 2, …, N_r) and wire diameter Φ_2, carrying filamentary circular concentric currents that have no magnetic substrate. The primary coil—with N_a concentric circular loops with different radii a_i (i=1, 2, …, N_a) and wire diameter Φ_1 located in a linear, homogeneous, and isotropic ferrite substrate—is characterized by μ_r, σ, and t. An AC voltage ($I_\Phi e^{j\omega t}$) was applied across the primary coil, and this induced an AC voltage on the secondary coil by the alternating magnetic field. As shown in Fig. 4, the system has cylindrical symmetry; the primary winding is placed at a distance $z=d_2$ (d_2 represents the distance between the primary winding and secondary substrate) from the ferrite substrate. From Maxwell's equations, the azimuthal electrical field created by the ith-turn of the primary winding at position (r, z) when $0<z\leq d_2$ was given by Hurley and Duffy (1997):

$$E_{\Phi,i}(r,z)=-\frac{j\omega\mu_0 I_\Phi a_i}{2}\int_0^\infty e^{-kd_2}\left[e^{kz}-\lambda(t)e^{-kz}\right]J_1(kr)J_1(ka_i)dk, \tag{7}$$

where I_Φ is the current amplitude (assumed to be sinusoidal), ω is the angular frequency, a_i is the radius of the ith-turn in the primary coil, and k is the integration variable. The parameter $\lambda(t)$ depends on the material properties and is defined as

$$\lambda(t)=\Phi(k)\frac{1-e^{-2\eta t}}{1-\Phi^2(k)e^{-2\eta t}}, \tag{8}$$

$$\Phi(k)=\frac{\mu_r-\eta/k}{\mu_r+\eta/k}, \tag{9}$$

$$\eta=\sqrt{k^2+j\omega\mu_r\mu_0\sigma}. \tag{10}$$

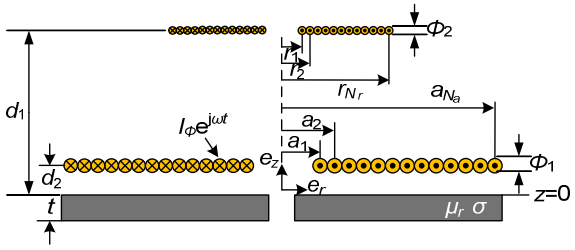

Fig. 4 Planar coils in a primary-substrate structure

The enhancement effect of the ferrite substrate on the self-inductance of the primary-substrate coil was investigated. In a linear, homogeneous, and isotropic problem, the total electrical field $E_\Phi(r, z)$ of the N_a-turn winding at (r, z) is the sum of the individual electrical fields created by the ith-turn expressed in Eq. (7). The total induced voltage at winding position $z=d_2$ is the sum of the voltage induced in each turn, which can be calculated by integrating $E_\Phi(r, z)$ along the winding length. It can be calculated as follows (Acero *et al*., 2006b):

$$\begin{aligned}V&=-\sum_{j=1}^{N_a}\sum_{i=1}^{N_a}\int_0^{2\pi}E_{\Phi,i}(r=a_j,z=d_2)a_j d\Phi\\&=-\sum_{j=1}^{N_a}\sum_{i=1}^{N_a}2\pi a_j E_{\Phi,i}(r=a_j,z=d_2).\end{aligned} \tag{11}$$

Therefore, the equivalent impedance of the primary coil on the ferrite substrate can be calculated using Eq. (12) and divided into equivalent resistive and inductive parts:

$$\begin{aligned}Z&=R_{eq}+j\omega L_{eq}=V/I_\Phi\\&=j\omega\mu_0\pi\int_0^\infty\left[1-\lambda(t)e^{-2kd_2}\right]T(k)dk,\end{aligned} \tag{12}$$

where L_{eq} and R_{eq} are the self-inductance and equivalent series resistance of the coil with ferrite substrate. The geometric function $T(k)$ is defined as

$$T(k)=2\sum_{i=1}^{N_a}\sum_{j>i}^{N_a}a_i a_j J_1(ka_i)J_1(ka_j)+\sum_{i=1}^{N_a}a_i^2J_1^2(ka_i). \tag{13}$$

Moreover, note that the inductive part L_{eq} in Eq. (12) can be divided into the inductance L of the winding, which would exist in the absence of the substrate, and the contribution of the substrate ΔL:

$$\Delta L=\pi\mu_0\int_0^{\infty}\text{real}\left[\lambda(t)\right]T(k)\text{e}^{-2kd_2}\text{d}k, \tag{14}$$

where real[$\lambda(t)$] is the real part of $\lambda(t)$ defined in Eq. (8). Thus, the total self-inductance L_t of the planar spiral coil on a ferrite substrate is the sum of Eqs. (5) and (14), and can be expressed as

$$L_\text{t}=L+\Delta L. \tag{15}$$

Following a similar analysis, the total electrical field at (r, z=d_1) can be expressed as

$$E_\Phi(r,z=d_1)=\sum_{i=1}^{N_a}E_{\Phi,i}(r,z=d_1), \tag{16}$$

where d_1 represents the distance between the secondary winding and secondary substrate. The total induced voltage in the secondary coil at (r, d_1) due to the primary coil at (r, d_2) is the sum of the voltage induced in each turn of the secondary coil:

$$\begin{aligned}V&=-\oint_{\text{secondary}}E_\Phi\cdot\text{d}l\\&=-\sum_{j=1}^{N_r}\int_0^{2\pi}E_\Phi(r=r_j,z=d_1)r_j\text{d}\Phi.\end{aligned} \tag{17}$$

Substituting Eq. (16) into Eq. (17) and replacing r with r=r_j in Eq. (16), we obtain

$$\begin{aligned}V&=-\sum_{i=1}^{N_a}\sum_{j=1}^{N_r}\int_0^{2\pi}E_{\Phi,i}(r=r_j,z=d_1)r_j\text{d}\Phi\\&=-\sum_{j=1}^{N_a}\sum_{i=1}^{N_a}2\pi r_jE_{\Phi,i}(r=r_j,z=d_1).\end{aligned} \tag{18}$$

Thus, the mutual impedance between the primary and secondary coils is

$$Z=\text{j}\omega M+Z_t=V/I_\Phi, \tag{19}$$

where M accounts for the mutual inductance between the coils, which would exist in the absence of the substrate, as expressed in Eq. (6), and Z_t accounts for the substrate:

$$\begin{aligned}Z_t&=R_\text{s}+\text{j}\omega\Delta M=\text{j}\omega\mu_0\pi\\&\cdot\sum_{i=1}^{N_r}\sum_{j=1}^{N_a}r_ia_j\int_0^{\infty}J_1(kr_i)J_1(ka_j)\lambda(t)\text{e}^{-k(d_1+d_2)}\text{d}k.\end{aligned} \tag{20}$$

In Eq. (20), R_s is the resistive component, which represents the losses due to the eddy current in the substrate, and ΔM is the inductive reactance which enhances the mutual inductance within the air-cored structure.

3.4 Sandwich structure

The addition of a secondary substrate that is characterized by μ_r, σ, and thickness t_1 above the secondary coil results in a sandwich structure (Fig. 5). From Maxwell's equations, the azimuthal electrical field created by the ith-turn of the primary winding at position (r, z) when $S-d_2\leq z\leq S-d_1$ (S represents the distance between the two substrates) was given by Hurley and Duffy (1997). In the same manner as described for the primary-substrate structure, we integrated the total N_a-turn electrical field at (r, z=$S-d_1$) induced by the carrying currents in the primary coil at (r, z=$S-d_2$) along the winding length of the secondary coil to obtain the individual induced voltage V_j (j=1, 2, …, N_r) in each turn. So, the total induced voltage V in a secondary coil is the sum of V_j. Then the mutual impedance Z between the primary and secondary coils can be calculated by V/I_Φ:

$$Z=\text{j}\omega M+Z_\text{sw}, \tag{21}$$

$$\begin{aligned}Z_\text{sw}&=R_\text{s}+\text{j}\omega\Delta M=\text{j}\omega\mu_0\pi\\&\cdot\sum_{i=1}^{N_r}\sum_{j=1}^{N_a}r_ia_j\int_0^{\infty}J_1(kr_i)J_1(ka_j)\left[f(\lambda)+g(\lambda)\right]\text{d}k,\end{aligned} \tag{22}$$

$$f(\lambda)=\frac{\lambda(t_1)\text{e}^{-k(d_1+d_2)}+\lambda(t_2)\text{e}^{-k(d_1'+d_2')}}{1-\lambda(t_1)\lambda(t_2)\text{e}^{-2kS}}, \tag{23}$$

$$g(\lambda)=\frac{2\lambda(t_1)\lambda(t_2)\text{e}^{-2kS}\cosh\left[k(d_2-d_1)\right]}{1-\lambda(t_1)\lambda(t_2)\text{e}^{-2kS}}, \tag{24}$$

$$d_1'=S-d_1,\quad d_2'=S-d_2. \tag{25}$$

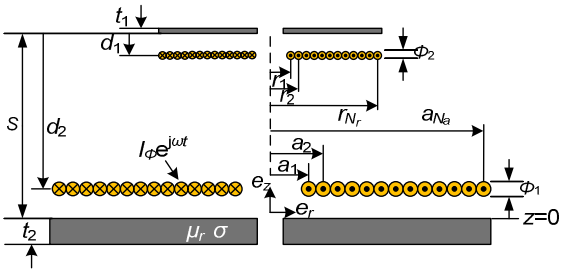

Fig. 5 Planar coils in a sandwich structure

4 FEA simulated model

Using ANSYS Maxwell v16.0 with a 3D magnetostatic solver to do the FEA simulations, we analyzed the self-inductance and the coupling relationship between the transmitter and receiver. The coils shown in Fig. 6a were modeled as two cylinders with 15 mm separation. The actual primary coil in the TET system has 19 turns of Litz wire made with 120 strands of American wire gauge (AWG) No. 42 corresponding to a wire diameter of 1.5 mm; the secondary coil has 20 or 30 turns of Litz wire made with 24 strands of AWG No. 42 wire corresponding to a wire diameter of 0.5 mm. Thus, from the Maxwell software, the primary coil was modeled as a cylinder with an outer radius of 32 mm, an inner radius of 2.5 mm, and a thickness of 5 mm, which is approximately equal to the radius of the actual Litz wire. A 19 ampere-turn current excitation characterized by the type of strands was added to the inflow face of the coil in the *XZ* plane. The secondary coil was modeled in the same way as the primary coil. The primary and secondary ferrite substrates were modeled according to the actual dimensions and properties (Table 2). The mesh of the primary and secondary coils in FEA contained 645 nodes and 287 nodes (in the primary substrate), and 514 nodes and 346 nodes (in the secondary substrate), respectively. The field calculator of the Maxwell program makes it possible to operate with primary magnetic flux density (***B***) and field intensity (***H***) around the structures according to the excitation current in each coil. This was achieved using vector algebra and calculus operations in a way that is both mathematically correct and meaningful from the perspective of Maxwell's equations (ANSYS, Inc., 2006). The self- and mutual inductances of the coils can also be defined by the energy storage which is determined by the magnetic flux density and field intensity in the solution space.

5 Comparative verification

5.1 Experimental setup

The analytical models and numerical simulations for determining the self- and mutual inductances of the planar Litz-wire coil with different structures were explained in the previous sections. To evaluate the validity of the formulas and FEA methods presented, variable prototypes (Figs. 3–5) were chosen as practical examples. The geometric and characteristic parameters of the primary and secondary planar spiral coils with air-cored structures are shown in Table 1. Two types of secondary windings with different numbers of turns for a fixed outer radius were tested and examined. Note that the ferrite material is brittle, especially when it is fabricated into thin plates. Thus, if the thickness is reduced, the allowable maximum size will shrink. In this paper, two ferrite plates of 5-mm and 1-mm thickness were used in the bottom of the primary and secondary winding, respectively. The detailed material properties of the ferrite substrate are shown in Table 2. Three types of TET links were constructed using fabricated planar spiral coils with Litz wire. Photos of the tested planar spiral coils and different cases are shown in Fig. 6a. Case 1 (P_{19air}+S_{30air}) and case 3 (P_{19air}+S_{20air}) represent the air-cored structure link discussed in Section 3.2; case 5 ($P_{19substrate}$+S_{30air}) and case 7 ($P_{19substrate}$+S_{20air}) represent the primary-substrate structure link described in Section 3.3; and case 6 ($P_{19substrate}$+$S_{30\ substrate}$) and case 8 ($P_{19substrate}$+$S_{20substrate}$) represent the sandwich structure link described in Section 3.4. P_{19air} and $P_{19substrate}$ represent primary coils with 19 turns wire

Table 1 Geometric parameters of the windings in a TET coil with air-cored structure

Parameter	P_{19}	S_{20}	S_{30}	Note
N	19	20	30	Number of turns
n_0	120	24	24	Number of strands
R_{in} (mm)	3.5	8.5	3.0	Coil inner radius
R_{out} (mm)	32	17.5	17.5	Coil external radius
Φ_c (mm)	0.06	0.06	0.06	Diameter of strand
Φ_o (mm)	1.5	0.5	0.5	Diameter of bundle
l	1	1	1	Number of layers

P_{19} represents primary coil with 19 turns wire; S_{20} and S_{30} represent secondary coils with 20 and 30 turns wire, respectively

Table 2 Material properties of the ferrite substrate

Parameter	Primary	Secondary	Note
t (mm)	5	1	Ferrite substrate thickness
R_{in} (mm)	2.5	2.5	Inner radius
R_{out} (mm)	32	17.5	External radius
μ_r	2500	2500	Relative permeability
σ $(\Omega\cdot m)^{-1}$	0.01	0.01	Conductivity

with air-cored and primary-substrate structures, respectively. S_{20air} and S_{30air} represent secondary coils with 20 and 30 turns wire with air-cored structure, respectively. $S_{20substrate}$ and $S_{30substrate}$ represent secondary coils with 20 and 30 turns wire with primary-substrate structure, respectively.

The practical self-inductances were determined by measuring the coils in practice with a HIOKI 3532-50 (HIOKI Company, Japan) impedance analyzer. The primary coil was fixed to an upholder, and the secondary coil was mounted on a 4D coordinate moving workbench (Fig. 6b). The relative position between the coil pair could be randomly adjusted. The axial distance between the coil pair would be about equal to the thickness of a patient's skin, fatty tissue, or muscle, nominally between 10 and 25 mm (Dissanayake *et al*., 2009). The primary coil was excited with an AC voltage (V_i) produced by a signal generator, and the secondary side voltage V_o was the open circuit voltage. The frequency was set at 256 kHz in this study, which is an operating frequency typical in a TET system. We opted for an easy way to measure the induced open voltage (V_o) at the secondary coil, and then determined the mutual inductance M with the following formula:

$$M = L_1 V_o / V_i . \tag{26}$$

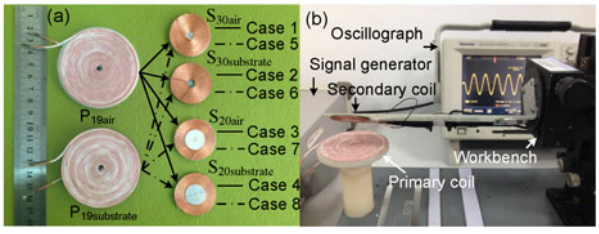

Fig. 6 Photograph of tested planar spiral coils and different cases (a) and the measurement system (b)

5.2 Self-inductances of coils

In the first test, the enhancement effect of the ferrite substrate on the self-inductance of the planar coil was studied. The measured results for the primary and secondary coils with different turns in air-cored and substrate structures were compared with FEA results (Table 3). The last two columns show percentage differences among the measured, simulated, and calculated values of L. The measured, simulated, and calculated results agree satisfactorily with each other and prove the validity of Eqs. (5) and (15). The contribution of the ferrite substrate to L is more than 63% of the total inductance for the three kinds of coil. This result agrees with previous studies examining the effects of planar inductors on magnetic substrates (Roshen and Turcotte, 1988). Some small errors of less than 4.4% can be found among the inductances from measurement, simulation, and calculation, which may be negligible with a better design or optimization of the coils.

Table 3 Comparison of L from experiment, simulation, and theory

Coil	L (μH)			Error (%)	
	M	S	C	M-S	M-C
P_{19air}	9.60	9.93	9.65	3.4	0.5
$P_{19substrate}$	17.16	16.76	17.05	2.3	0.6
S_{30air}	18.13	17.53	18.39	3.3	1.4
$S_{30substrate}$	29.21	29.79	28.69	2.0	1.8
S_{20air}	12.76	12.81	12.72	0.4	0.3
$S_{20substrate}$	21.38	21.21	20.44	0.8	4.4

M: measured result; S: simulated result; C: calculated result. The errors between M-S and M-C are computed according to formulas |(S−M)/M| and |(C−M)/M|, respectively

The parameter $\lambda(t)$, which depends on material properties in Eq. (8), contains four variables relating to the substrate of interest: t, μ_r, σ, and the frequency f. The frequency-dependent eddy current loss induced in the substrate, which dissipates some of the energy generated in the winding, becomes evident when the skin depth is small because of the high operating frequency and conductivity. Fig. 7a shows that the magnetic substrate does not significantly influence the winding inductance with the increase of frequency. Fig. 7b shows the inductance enhancement as a function of relative permeability for different values of substrate thickness. Note that the enhancement effect of the substrate is directly proportional to its thickness and relative permeability; however, the contribution to the inductance of the substrate will reach a saturation point when the relative permeability increases to a certain point. The same relationship was found between the inductance enhancement and the substrate thickness for different values of relative permeability (Fig. 7c). A greater saturation level and corresponding enhancement effect will be achieved for a thickness with a higher value of relative

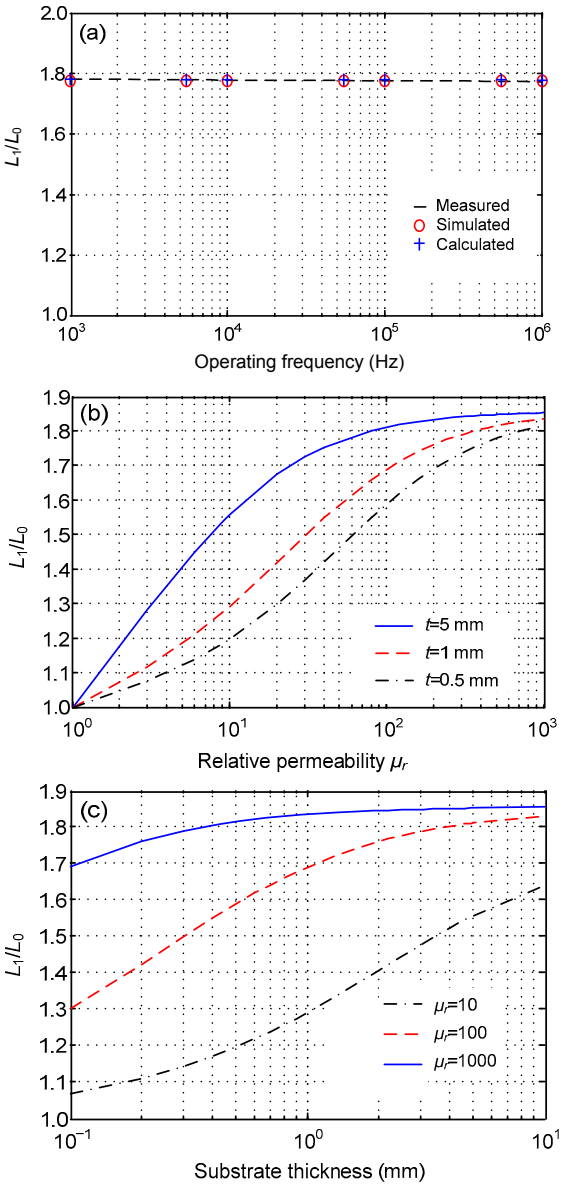

Fig. 7 Enhancement of calculated self-inductance L_1 ($P_{19substrate}$) with ferrite substrate (simulated results) when L_0=9.649 μH (P_{19air})

(a) As a function of operating frequency f (μ_r=1000, t=5 mm); (b) As a function of μ_r (f=256 kHz); (c) As a function of t (f=256 kHz)

permeability. The overall enhancement satisfies $1 \le L_1/L_0 \le 1.85$.

5.3 Mutual inductances between coils

To analyze M numerically, 3D FEA simulations of different TET cases were performed in Maxwell v.16. To predict M analytically, some analytical models were employed using the parameters shown in Tables 1 and 2. Here, the axial distance ranged from 5 to 25 mm, visualizing the applicable area of the model. The mutual inductance curves as functions of axial separation for case 1 (air-cored structure) and case 5 (primary-substrate structure) with a secondary coil of 30 turns are plotted in Fig. 8a. Eq. (6) was used for analytical prediction of M in case 1. To calculate the enhanced mutual inductance ΔM due to the contribution of the substrate, Eq. (20) was employed in this model. The measured enhanced mutual inductance (ΔM measured) can be calculated by subtracting the measured results of case 1 from those of case 5. The simulated enhanced mutual inductance (ΔM simulated) can be obtained in the same way. The agreement among the measured, calculated, and simulated results is very good in all cases. Expressions (6) and (20) can easily predict M and ΔM, respectively. The results in Fig. 8a indicate that the mutual inductance between the primary and secondary coils can be enhanced when ferrite substrate is used, and will reduce with the increase of axial distance. The comparison among the measured, calculated, and simulated results in Fig. 8b shows that the error between the calculated and measured results for case 1 is limited to 5%. The simulated results for cases 1 and 5 were also compared with the measurement results, and the error is limited to 8.2%. The maximum error among the measured, calculated, and simulated ΔM for case 5 is less than 15%.

Another investigation was made for a secondary coil of 20 turns, while the other parameters of the primary and secondary windings remained identical. The measured mutual inductance curves as functions of axial separation for case 3 (air-cored structure) and case 7 (primary-substrate structure) were compared with simulated and calculated results in Fig. 8c. The measured, simulated, and calculated results agreed satisfactorily and prove the validity of the formulas. Moreover, the comparison in Fig. 8d shows that the error between the calculated and measured results is limited to 5%, and the errors between the simulated and measured results for both cases 3 and 7 are limited to 8%. The maximum error among the measured, calculated, and simulated ΔM for case 7 is limited to 16%.

The same investigation was made for cases 6 and 8, which represent a sandwich structure with a secondary coil of 30 and 20 turns, respectively, by

comparing the proposed model with measured and simulated results. Figs. 9a and 9c show the measured, simulated, and calculated results for cases 6 and 8, respectively, at different axial separations. Eq. (22) was employed to calculate ΔM for these cases using the parameters specified in Tables 2 and 3. The measured, simulated, and calculated results were compared in Figs. 9b and 9d, and the error is limited to 12%.

In Figs. 8 and 9, some differences in error rates can be found among the measured, simulated, and calculated values of mutual inductance for all cases. There are four analytical approximations that could account for these errors. First, in the analysis of the mutual inductance, the carrying current density of every turn is assumed to be constant. However, because the inside path for current flow is shorter than the outside edge, the resistance is reduced on the inside with consequential higher current density. Moreover, the current density over the cross-sectional area of the trace is redistributed due to the skin and a proximity effect at high frequency, as discussed in Section 3.1. Due to the large magnetic field intensity or high operating frequency, additional unevenness exists. Thus, the calculation errors depend on the operating frequency and the distance between the coils. For a TET system, in which the typical values of frequency and axial distance are several hundred kHz and a few mm, respectively, the formulas can give an acceptable prediction of the mutual inductance. Second, the analytical model is based on the assumption that the ferrite substrate is infinite in the radial direction. However, in practical measurements, the size of the substrate is the same as the diameter of the coil. The air gap and fringing effects due to the finite substrate cannot be totally removed. Therefore, small errors are observed in Figs. 8 and 9. Third, the difference between the measured and simulated coupling coefficients is likely due to a combination of measurement error and the assumption that the coils are constructed from solid copper wire in the simulated model. However, the real coil winding consists of Litz wire, which incorporates air gaps between the strands that form the windings and also some cancellation of the magnetic field in each strand due to its vicinity to other strands as well as in each turn (caused by other

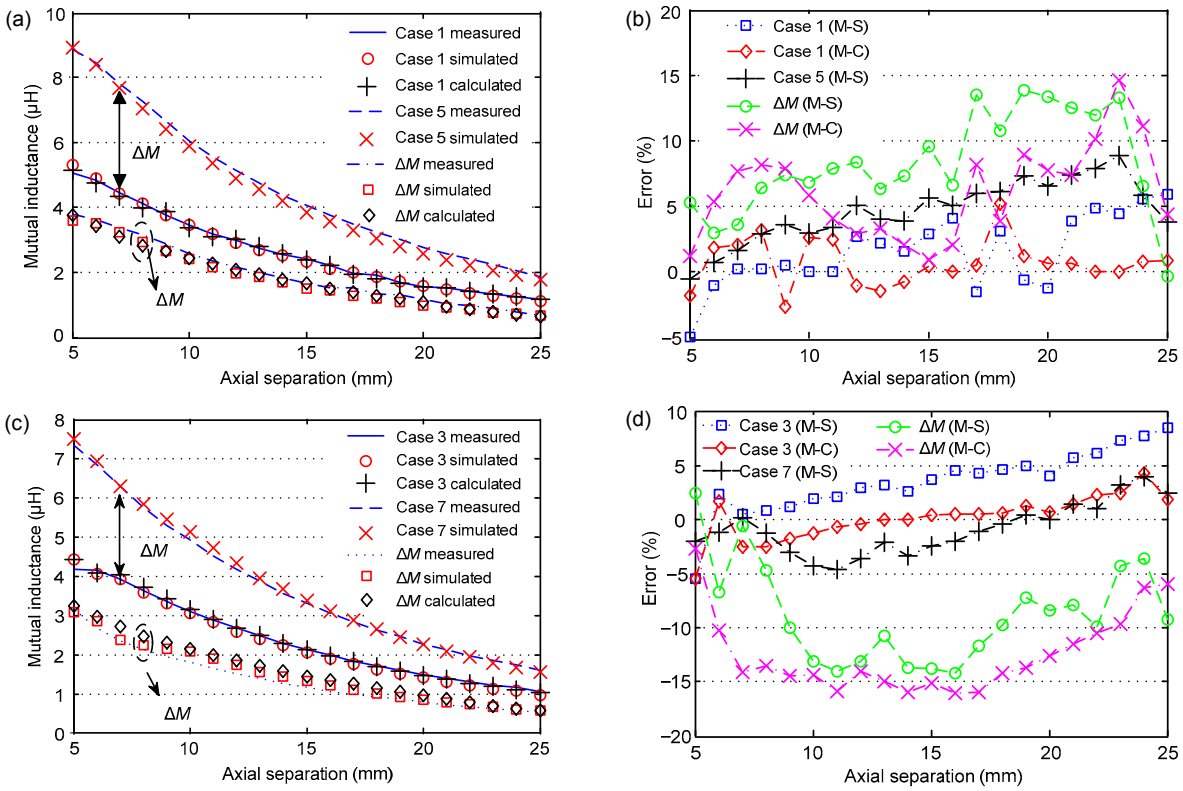

Fig. 8 Measured, simulated, and calculated mutual inductance M for four cases in a primary-substrate structure
(a) M for cases 1 and 5; (b) Comparison of M for cases 1 and 5; (c) M for cases 3 and 7; (d) Comparison of M for cases 3 and 7

turns of the winding). Lastly, it is difficult to manufacture identical Litz wire with a high number of strands. Normally strands are twisted instead of plaited by hand for the secondary winding. In other words, the wire diameter of each turn could not be guaranteed to be constant. Thus, in prototype tests as compared to the analytical model, the actual dimension distribution in each turn of winding is neither valid nor even.

As in the previous analysis, the mutual inductance curve dropped gradually as the primary and secondary coils moved apart from each other. Thus, the detrimental effect of axial separation on the mutual inductance and transfer efficiency is prominent. As a result, a pair of coils whose characteristics can create a relatively smooth mutual inductance curve will be preferred in a TET system, to reduce the variability of the transfer characteristics. For a given footprint area (i.e., the outermost radius is fixed), the magnetic flux distribution of a planar spiral winding depends on the winding geometry and structure. The mutual inductance curves of six cases that represent different winding geometry and structure at different axial separations are plotted in Fig. 10. The geometry of the primary winding is kept identical in all cases. A smoother and optimal curve could be obtained from a secondary winding with a large number of turns and a sandwich structure. The magnetic field intensity between the coils would be improved by the ferrite substrates on the primary and secondary windings.

5.4 Coupling coefficients of coils

To simplify the transfer efficiency equations, Babic *et al*. (2011) normalized M with regard to the primary inductance (L_1) and secondary inductance (L_2) by defining k as the coupling coefficient between the coils:

$$k = M / \sqrt{L_1 L_2}\,. \tag{27}$$

Fig. 11 illustrates the effect on the coupling coefficient when the axial separation was increased from 5 to 25 mm for three link structures. The measured, calculated, and simulated results can be calculated

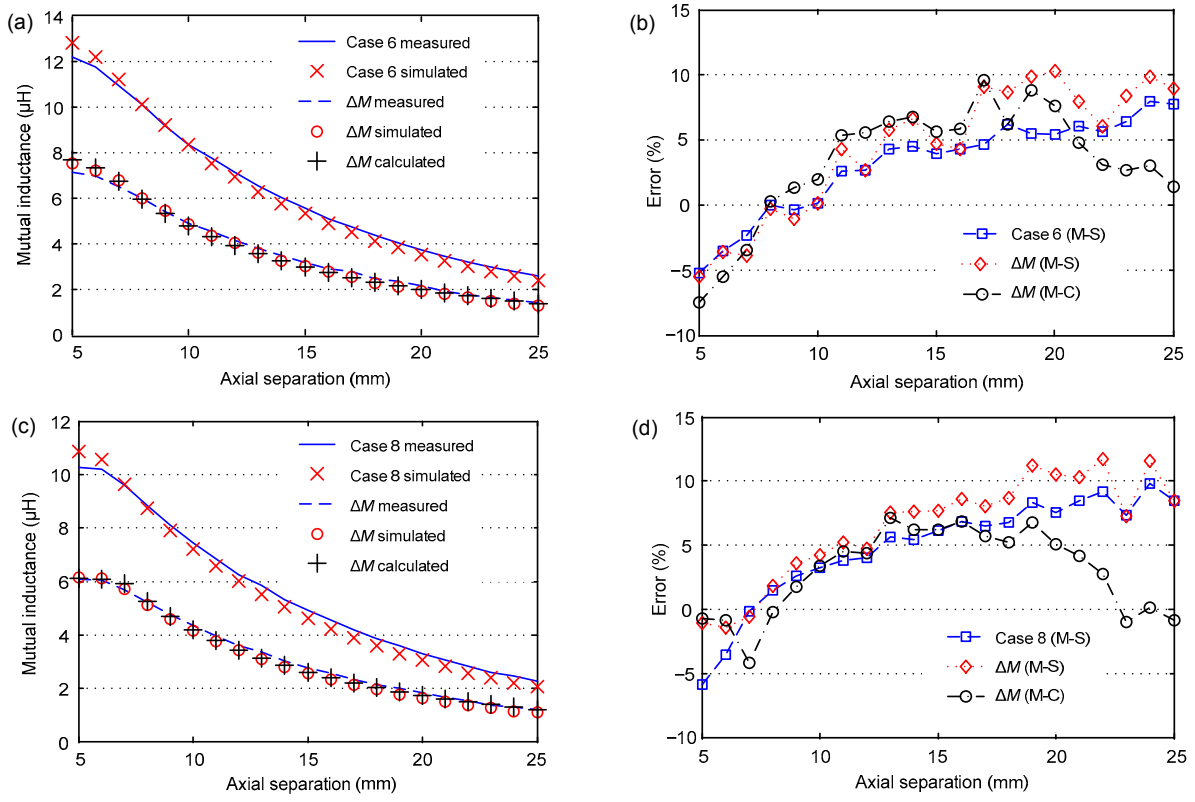

Fig. 9 Measured, simulated, and calculated mutual inductance M for four cases in a sandwich structure
(a) M for case 6; (b) Comparison of M for case 6; (c) M for case 8; (d) Comparison of M for case 8

using Eq. (27) based on the corresponding values of M and L from the three methods. As expected, with the coils aligned axially, the coupling coefficient decreases as the separation increases. All three methods produced consistent results. The calculated and simulated k for different cases were compared with the measured results at 15-mm axial distance (Table 4); the simulated coupling coefficient was within 3.7% of the measured result and the calculated result was within 3.0% of the measured result.

Results from the figures show that a higher and smoother coupling strength can be obtained from windings with a small number of turns placed near the edge of the winding area over the entire structure. Furthermore, significant enhancement of the coupling coefficient can be achieved using ferrite substrate. This is an important observation in planar spiral winding design. Because the outermost radii of the primary and secondary windings in all cases have been fixed, a type of winding with an optimal innermost radius is needed to obtain the best coupling coefficient. An explanation for this observation could be the magnetic flux distribution associated with the innermost radius of the winding (Liu and Hui, 2008). The magnetic field intensity of the winding with a smaller inner radius is highest in the central region and drops quickly from the center to the periphery of the spiral winding. In contrast, the magnetic field distribution of the winding with a relatively large

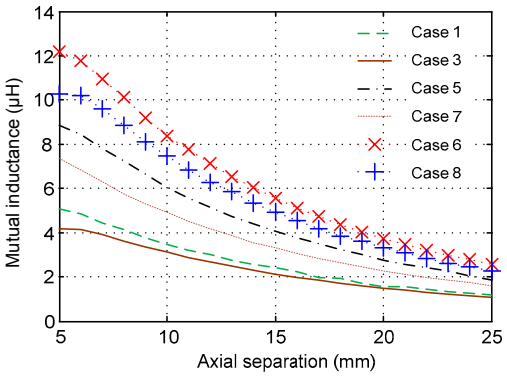

Fig. 10 Measured, simulated, and calculated mutual inductance M for the six cases

Table 4 Comparison of k from experiment, simulation and theory (axial distance=15 mm)

Case	k			Error (%)	
	M	S	C	M-S	M-C
1	0.182	0.178	0.179	2.2	1.6
3	0.193	0.186	0.191	3.6	1.0
5	0.231	0.223	0.228	3.5	1.3
6	0.248	0.239	0.242	3.6	2.4
7	0.233	0.228	0.240	2.1	3.0
8	0.257	0.251	0.253	2.3	1.6

M: measured; S: simulated; C: calculated. The errors between M-S and M-C are computed according to formulas |(S−M)/M| and |(C−M)/M|, respectively

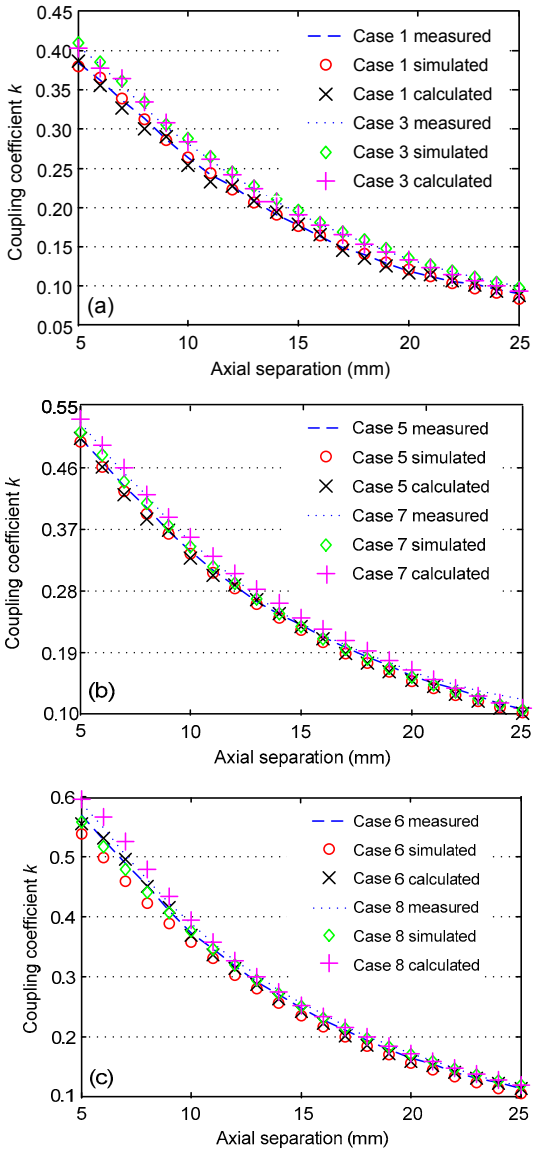

Fig. 11 Measured, simulated, and calculated coupling coefficients k of three different coil structures

(a) Air-cored structure (cases 1 and 3); (b) Primary-substrate structure (cases 5 and 7); (c) Sandwich structure (cases 6 and 8)

innermost radius decreases evenly and slowly from the periphery to the center.

In case 8 ($P_{19substrate}$+$S_{20substrate}$), the impact of the thickness and relative permeability of the ferrite substrate on coupling is shown in Fig. 12. Fig. 12a illustrates the calculated coupling curve as a function of the thickness of the primary substrate for different thicknesses of the secondary substrate. Here, the axial separation was fixed at 15 mm and the relative permeability was 1000. For clear comparison, all of the coupling coefficient results were normalized with the value k_0 in the corresponding air-cored structure (case 3). When the thickness of the secondary substrate was fixed at t_2=1 mm, and if the thickness of the primary substrate was more than a critical value (e.g., t_1=1.9 mm), then the enhancement effect of the primary ferrite substrate on the coupling coefficient is kept at a nearly constant value as the primary substrate's thickness increases (Fig. 12a). Because of the limited space under the patients' skin, in practical applications, the thickness of the secondary ferrite substrate is usually t_2=1 mm. Fig. 12b shows the enhancement ratio of the coupling coefficient as a function of the permeability of the ferrite substrate for two thickness combinations (t_1=5 mm, t_2=1 mm and t_1=2 mm, t_2=1 mm). Results indicate that the coupling strength can be enhanced as the relative permeability of the ferrite substrate increases. However, if the permeability is increased to a certain critical value (e.g., μ_r=1000), the enhancement effect on coupling due to the ferrite plate will reach a saturation point.

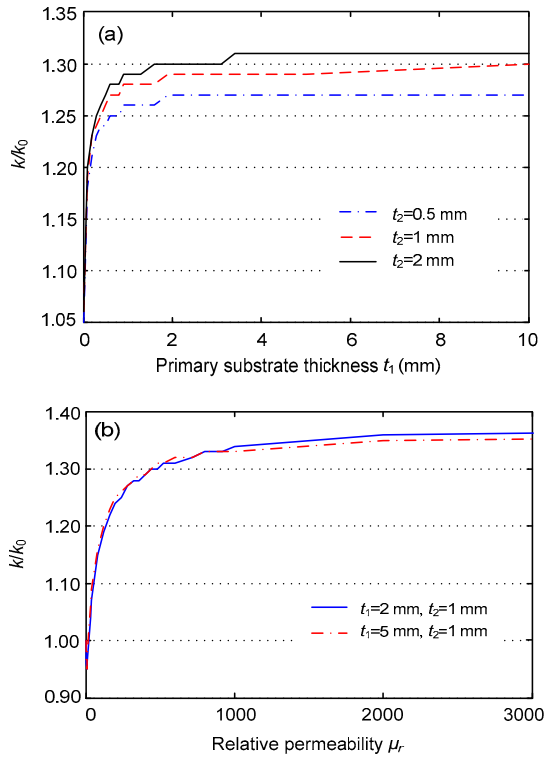

Fig. 12 Enhancement of coupling coefficient k for case 8 (calculated results) at 15-mm axial distance (k_0=0.186)
(a) As a function of t_1; (b) As a function of μ_r

6 Conclusions

The first focus of this paper was on the development of a novel elastic scaling artificial anal sphincter prosthesis composed of an annular elastic mechanism and a shrinkable actuator. Compared with existing technologies, the simplicity and automation of our prosthesis make it a good candidate for patients with severe FI. As an important part of the system, magnetic coupling analysis of TET coils was carried out for circuit design and optimization applications. A series of formulas for two coaxial planar spiral windings with Litz wire in three kinds of structures were established and compared with FEA and practical measurements. The agreement among the measured, calculated, and simulated results was good in all cases. These formulas were based on the physical dimensions of the windings and the electromagnetic properties of the ferrite substrate. We found that these analytical models could be used to obtain the optimal value of magnetic coupling between the coils, critical values of the relative permeability, thickness of the ferrite substrate for a given material, as well as the innermost radius of the coil for a fixed outermost radius. This is useful for optimizing the geometric design of windings and the ferrite substrate in a sandwich structure. In addition to providing design insight, the analysis allows system efficiency-optimizing schemes to be developed.

References

Acero, J., Alonso, R., Burdio, J.M., *et al*., 2006a. Analytical equivalent impedance for a planar circular induction heating system. *IEEE Trans. Magn.*, **42**(1):84-86. [doi:10.1109/TMAG.2005.854443]

Acero, J., Alonso, R., Burdio, J.M., *et al*., 2006b. Frequency-dependent resistance in Litz-wire planar windings for domestic induction heating appliances. *IEEE Trans.*

Power Electron., **21**(4):856-866. [doi:10.1109/TPEL.2006.876894]

ANSYS, Inc., 2006. Ansoft Maxwell 3D Field Simulator v11 User's Guide (Ansoft Corporation, Rev. 2.0).

Babic, S., Sirois, F., Akyel, C., *et al*., 2010. Mutual inductance calculation between circular filaments arbitrarily positioned in space: alternative to grover's formulas. *IEEE Trans. Magn.*, **46**(9):3591-3600. [doi:10.1109/TMAG.2010.2047651]

Babic, S., Sirois, F., Akyel, C., *et al*., 2011. New formulas for mutual inductance and axial magnetic force between a thin wall solenoid and a thick circular coil of rectangular cross-section. *IEEE Trans. Magn*., **47**(8):2034-2044. [doi:10.1109/TMAG.2011.2125796]

Belyaev, O., Müller, C., Uhl, W., 2006. Neosphincter surgery for fecal incontinence: a critical and unbiased review of the relevant literature. *Surg. Today*, **36**(4):295-303. [doi:10.1007/s00595-005-3159-4]

Bharucha, A.E., Wald, A., Enck, P., *et al*., 2006. Functional anorectal disorders. *Gastroenterology*, **130**(5):1510-1518. [doi:10.1053/j.gastro.2005.11.064]

Conway, J.T., 2007. Inductance calculations for noncoaxial coils using Bessel functions. *IEEE Trans. Magn.*, **43**(3):1023-1034. [doi:10.1109/TMAG.2006.888565]

Dissanayake, T.D., Hu, A.P., Malpas, S., *et al.*, 2009. Experimental study of a TET system for implantable biomedical devices. *IEEE Trans. Biomed. Circ. Syst.*, **3**(6):370-378. [doi:10.1109/TBCAS.2009.2031539]

Edden, Y., Wexner, S.D., 2009. Therapeutic devices for fecal incontinence: dynamic graciloplasty, artificial bowel sphincter and sacral nerve stimulation. *Expert Rev. Med. Device*, **6**(3):307-312. [doi:10.1586/erd.09.10]

Gallas, S., Leroi, A.M., Bridoux, V., *et al*., 2009. Constipation in 44 patients implanted with an artificial bowel sphincter. *Int. J. Colorectal Dis.*, **24**(8):969-974. [doi:10.1007/s00384-009-0693-3]

Grover, F.W., 1962. Inductance Calculations. Dover Publications, NY, USA.

Hurley, W.G., Duffy, M.C., 1997. Calculation of self- and mutual impedances in planar sandwich inductors. *IEEE Trans. Magn.*, **33**(3):2282-2290. [doi:10.1109/20.573844]

Jow, U.M., Ghovanloo, M., 2007. Design and optimization of printed spiral coils for efficient transcutaneous inductive power transmission. *IEEE Trans. Biomed. Circ. Syst.*, **1**(3):193-202. [doi:10.1109/TBCAS.2007.913130]

Lee, S.H., Lorenz, R.D., 2011. Development and validation of model for 95%-efficiency 220-W wireless power transfer over a 30-cm air gap. *IEEE Trans. Ind. Appl.*, **47**(6):2495-2504. [doi:10.1109/TIA.2011.2168555]

Liu, X., Hui, S.Y.R., 2008. Optimal design of a hybrid winding structure for planar contactless battery charging platform. *IEEE Trans. Power Electron.*, **23**(1):455-463. [doi:10.1109/TPEL.2007.911844]

Ma, G.Y., Yan, G.Z., He, X., 2007. Power transmission for gastrointestinal microsystems using inductive coupling. *Physiol. Meas.*, **28**(3):9-18. [doi:10.1088/0967-3334/28/3/N01]

Ma, J.M., Yang, Q.X., Chen, H.Y., 2010. Transcutaneous energy and information transmission system with optimized transformer parameters for the artificial heart. *IEEE Trans. Appl. Supercond.*, **20**(3):798-801. [doi:10.1109/TASC.2010.2043241]

Mohan, S.S., Hershenson, M.M., Boyd, S.P., *et al*., 1999. Simple accurate expressions for planar spiral inductors. *IEEE J. Solid-State Circ.*, **34**(10):1419-1424. [doi:10.1109/4.792620]

Mundy, L., Merlin, T.L., Maddern, G.J., *et al*., 2004. Systematic review of safety and effectiveness of an artificial bowel sphincter for faecal incontinence. *Brit. J. Surg.*, **91**(6):665-672. [doi:10.1002/bjs.4587]

RamRakhyani, A.K., Mirabbasi, S., Chiao, M., 2011. Design and optimization of resonance-based efficient wireless power delivery systems for biomedical implants. *IEEE Trans. Biomed. Circ. Syst.*, **5**(1):48-63. [doi:10.1109/TBCAS.2010.2072782]

Roshen, W.A., Turcotte, D.E., 1988. Planar inductor on magnetic substrates. *IEEE Trans. Magn.*, **24**(6):3213-3216. [doi:10.1109/20.92379]

Soma, M., Galbraith, D.C., White, R.L., 1987. Radio-frequency coils in implantable devices: misalignment analysis and design procedure. *IEEE Trans. Biomed. Eng.*, **34**(4):276-282. [doi:10.1109/TBME.1987.326088]

Wong, D.W., Congliosi, S.M., Spencer, M.P., *et.al.*, 2002. The safety and efficacy of the artificial bowel sphincter for fecal incontinence. *Dis. Colon Rectum*, **45**(9):1139-1153. [doi:10.1007/s10350-004-6381-z]

Yue, C.P., Wong, S.S., 2000. Physical modeling of spiral inductors on silicon. *IEEE Trans. Electron Device*, **47**(3):560-568. [doi:10.1109/16.824729]

Zan, P., Yan, G., Liu, H., 2008. Modeling of human colonic blood flow for a novel artificial anal sphincter system. *J. Zhejiang Univ.-Sci. B (Biomed. & Biotechnol.)*, **9**(9):734-738. [doi:10.1631/jzus.B0820099]

Zan, P., Yan, G., Liu, H., 2009a. Analysis of electromagnetic compatibility in biological tissue for a novel artificial anal sphincter. *IET Sci. Meas. Technol.*, **3**(1):22-26. [doi:10.1049/iet-smt:20080063]

Zan, P., Yan, G., Liu, H., *et al*., 2009b. Adaptive transcutaneous power delivery for an artificial anal sphincter system. *J. Med. Eng. Technol.*, **33**(2):136-141. [doi:10.1080/03091900801943205]

Zhang, X., Ho, S.L., Fu, W.N., 2011. Quantitative analysis of a wireless power transfer cell with planar spiral structures. *IEEE Trans. Magn.*, **47**(10):3200-3203. [doi:10.1109/TMAG.2011.2147768]

Zierhofer, C.M., Hochmair, E.S., 1996. Geometric approach for coupling enhancement of magnetically coupled coils. *IEEE Trans. Biomed. Eng.*, **43**(7):708-714. [doi:10.1109/10.503178]